

A potential broad-spectrum neutralizing antibody against Betacoronavirus

Rong Wang¹ | Jiazheng Guo¹  | Jiansheng Lu¹ | Peng Du¹ | Jun Zhang¹ | Yunzhou Yu¹ | Lei Chen¹ | Zhiqi Xiong² | Yuning Xiang² | Xiaodan Ni² | Junjie Xu¹ | Zhixin Yang¹

¹Beijing Institute of Biotechnology, Beijing, China

²Shuimu BioSciences Co., Ltd, Beijing, China

Correspondence

Zhixin Yang and Junjie Xu, Dongda St No. 20, Fengtai District, Beijing, China.

Email: yy_xiao@126.com and xujunjie@sina.com

Abstract

Three pandemics caused by human Betacoronavirus had broken out in the past two decades. Severe acute respiratory syndrome coronavirus-2 (SARS-CoV-2) was one of the novel epidemic strains which caused the third pandemic, coronavirus disease 2019 (COVID-19), a global public health crisis. So far, more than millions of people have been infected. Considering the public health and economic impact of Betacoronavirus pandemic, drugs with broad-spectrum activity against these coronaviruses are urgently needed. In this study, two monoclonal antibodies targeting SARS-CoV-2 spike protein receptor-binding domain (RBD) with good neutralizing activity were used to construct a novel immunoglobulin-like bispecific antibody BI31. The neutralizing effect of BI31 against the pseudovirus and the authentic virus is better than that of its parent antibodies alone and in combination. What surprised us most was that the newly constructed bispecific antibody also had the neutralizing activity against SARS-CoV and Middle East respiratory syndrome coronavirus (MERS-CoV) that the parent antibodies did not have. These suggested that the BI31 can not only be developed as a therapeutic drug against COVID-19 but it could also become a broad-spectrum therapeutic antibody against Betacoronavirus.

KEYWORDS

antibody neutralization, Betacoronavirus, bispecific antibody, broad-spectrum antibody, SARS-CoV-2

1 | INTRODUCTION

Coronaviruses are zoonotic pathogens and infect a wide variety of host organisms. Coronaviruses can be divided into Alphacoronavirus, Betacoronavirus, Gammacoronavirus, and Deltacoronavirus genera based on their genomic structures. At present, seven

human-susceptible coronaviruses have been found, two species of the Alphacoronavirus genus (HCoV-229E, HCoV-NL63), and five species of the Betacoronavirus genus (SARS-CoV, MERS-CoV, SARS-CoV-2, HCoV-OC43, and HCoV-HKU1). Among them, all three highly pathogenic coronaviruses belong to Betacoronavirus genus, which were severe acute respiratory syndrome coronavirus

Rong Wang and Jiazheng Guo contributed equally to this work.

This is an open access article under the terms of the [Creative Commons Attribution-NonCommercial-NoDerivs](https://creativecommons.org/licenses/by-nc-nd/4.0/) License, which permits use and distribution in any medium, provided the original work is properly cited, the use is non-commercial and no modifications or adaptations are made.

© 2023 The Authors. *Journal of Medical Virology* published by Wiley Periodicals LLC.

(SARS-CoV) in 2002, Middle East respiratory syndrome coronavirus (MERS-CoV) in 2014, and severe acute respiratory syndrome coronavirus 2 (SARS-CoV-2) in 2019, and SARS-CoV-2 has caused a global pandemic.¹

Coronaviruses are single-stranded, positive-sense RNA virus with a genome of approximately 30 kb. Coronaviruses consist of internal genetic material RNA and spike protein S, envelope membrane protein E, membrane protein M, and nucleocapsid protein N.²⁻⁵ Among them, spike (S) glycoprotein promotes viral entry into host cells through an S1 subunit whose receptor-binding domain (RBD) bind to receptor (ACE2 or DPP4) and an S2 subunit mediating membrane fusion.^{6,7} The main manifestations after virus infection are fever or mild cough; patients with severe illness can develop pneumonia, which is often accompanied by organ failure and even death.⁸⁻¹⁰

Effective means of prevention and treatment are urgently needed to control COVID-19. Currently, Different kinds of vaccines—including inactivated vaccine, mRNA vaccine, and recombinant vaccine, have been successfully developed for the prevention of COVID-19 infection, and several small molecule drugs, such as Paxlovid, have been approved for emergency use.¹¹⁻¹³ However, existing studies have shown that the vaccine can only prevent severe cases, but not avoid infection, and the ultimate effect of chemical drugs needs further clinical verification.¹⁴ Therefore, specific treatments are still urgently needed. Neutralizing antibody plays an important role in the prevention and treatment of viral infection. Studies have shown that some anti-COVID-19 antibodies compete with ACE2 to bind to RBD and prevent the virus from infecting host cells.¹⁵⁻¹⁸ Earlier, several antibody drugs were being developed as COVID-19 treatments, such as Lilly's LY-CoV555 and Kingstone's JS016, both of which received emergency use authorizations from the US Food and Drug Administration.^{19,20} However, RBD mutation caused that the antibody reduced or even lost the neutralizing activity of the antibodies mentioned above against COVID-19. The combination of multiple antibodies is an effective means to effectively deal with the mutation of the target pathogen.²¹

Bispecific antibody (BsAb) is an emerging antibody drug. Unlike mAbs, BsAbs can bind two different antigenic molecules or two epitopes of one antigen. Their unique specificity and bifunctionality will make them a hot spot in antibody drug research and development once they have been launched. BsAbs have a wide range of applications in treating tumors and autoimmune diseases.^{22,23} Daniel Ruzek's group constructed a BsAb against SARS-CoV-2 in the CrossMAb format and detected a good neutralizing effect.²⁴ The anti-SARS-CoV-2 BsAb of VHH-Fc constructed by Professor Jianbo Dong's team has also achieved impressive research results.²⁵ This indicates that BsAbs are an effective treatment method in response to COVID-19.

Through preliminary work of using antibody display technology, a panel of chimeric human-mouse neutralizing antibodies was generated and characterized in our lab; some mAbs exhibited favorable biological activity in vitro for the inhibition of viral entry into host cells and neutralizing SARS-CoV-2.²⁶ Two humanized mAbs (SFC3 and HSA-1F) with good neutralizing activity and a certain synergistic effect were

chosen to construct the BsAb BI31. In the in vitro neutralization experiment, BI31 showed better neutralizing activity than the parental antibody and parental antibody cocktail. Furthermore, it also showed neutralizing activity against SARS-CoV-2-homologous SARS-CoV and MERS-CoV, which means that it may become a universal treatment that can be used for preventing and treating infection by other coronaviruses.

2 | MATERIALS AND METHODS

2.1 | Bispecific antibody construction and purification

The VH and VL of the mAbs SFC3 and HSA-1F were synthesized using custom gene synthesis. The HSA-1F VH and VL fragments were cloned into human heavy chain expression vector (containing CH1, CH2, and CH3) and human light chain expression vector (containing VL) by PCR and double enzyme digestion. To create BsAbs in the scFv-IgG format, the carboxyl terminus of the SFC3 VH and VL was fused with the amino terminus of the HSA-1F VH and VL by PCR and restriction digestion. For BsAb expression, two plasmids containing recombinant light and heavy chains, respectively, were cotransfected into FreeStyle 293-F cells (Invitrogen) with FectoPRO transfection reagent (116-001, Polyplus-transfection, FRA). After 72 h, the cell suspension was centrifuged at 8000 rpm for 10 min, the cell pellet was discarded, and the supernatants were collected. The antibody-containing supernatants were purified using HiTrap MabSelect SuRe (GE Healthcare) and desalted in pH 7.4 PBS (phosphate-buffered saline) solution using HiTrap Desalting (GE Healthcare). Finally, the purified antibody was analyzed by 10% sodium dodecyl sulfate-polyacrylamide gel electrophoresis (SDS-PAGE) (M00668, Gen-script, CHN) under reducing and nonreducing conditions, followed by staining with QuickBlue (BF06152, Biodragon, CHN) and was quantified by absorbance at 280 nm wavelength (A_{280}).

2.2 | Cell lines and pseudovirus packing

Huh7 cells and Vero E6 cells (ATCC) were cultured in Dulbecco's modified Eagle's medium (DMEM, Gibco) with 10% fetal bovine serum (FBS). FreeStyle™ 293-F cells (Invitrogen) were cultured in FreeStyle 293 Expression Medium (12338; Gibco). All cells were cultured at 37°C in 5% CO₂; the Huh7 cells were adherent cultures, and the FreeStyle™ 293-F cells were suspension cultures at 125 rpm. The gene encoding the SARS-CoV-2 S protein with 19 amino acids removed (GenBank NC_045512.2) was inserted into pcDNA3.1(+) (Invitrogen, V79020) yielding the plasmid pcDNA3.1-S-ST19. The pseudovirus required for the neutralization experiment was coated with HIV backbone vector pNL4-3.Luc.R-E- and pcDNA3.1-S-ST19. The eukaryotic expression plasmids of pNL4-3.Luc.R-E- and pcDNA3.1-S-ST19 were co-transfected into the FreeStyle™ 293-F cells at a ratio of 3:1 using FectoPRO transfection reagent. After 72 h, the FreeStyle™ 293-F cell suspension was centrifuged at 3000 rpm at

4°C for 30 min to collect the supernatant containing the virus particles. The obtained pseudovirus was separated into aliquots and stored at -80°C. The mutant pseudovirus had the same packaging work as the original strain, and the sequence mutation was completed by the Fast Mutagenesis System (FM111, TransGen Biotech, CHN).

2.3 | Enzyme-linked immunosorbent assay (ELISA)

The RBD protein was coated onto ELISA plates (9018, Costar); the RBD protein was diluted to 2 ng/μL with carbonate buffer. The coated plates were incubated at 4°C overnight, following which 200 μL 2% skimmed milk in PBS was added to each well and incubated at 37°C for 2 h to block nonspecific binding. From their initial concentration, the BsAb and parent mAb antibody solutions were serially diluted in blocking buffer, respectively, and then 100 μL from each concentration was added to separate wells and incubated at 37°C for 1.5 h. Subsequently, the ELISA plates were washed six times with PBS-Tween (0.1% v/v) and incubated at 37°C for 1 h in goat anti-human immunoglobulin G (IgG) horseradish peroxidase-conjugated antibody (1:4000, v/v). After washing the ELISA plate with PBS-Tween (0.1% v/v) six times again, the chromogen substrate o-phenylenediamine (OPD) was used for detection and the results were obtained at a wavelength of 492 nm.

2.4 | Pseudovirus-based neutralization assay

The antibodies were diluted threefold serially with DMEM for culturing Huh7 cells in a 96-well plate (40 μL per well). Pseudovirus was added to each well, and the 96-well plate containing the pseudovirus-antibody suspension was incubated at 37°C for 1 h to reach equilibrium. Huh7 cells expressing ACE2 (4×10^5 cells/mL, 40 μL per well) were seeded in each pseudovirus-antibody suspension well. After 40-h incubation at 37°C with 5% CO₂, the Huh7 cells were lysed and the luminescence was measured with a Luciferase Assay System (E1501, Promega). The median effective concentrations (EC₅₀) were calculated using nonlinear curve fitting in GraphPad Prism 8 (GraphPad Inc.).

2.5 | Determination of the binding capacity

The binding capacity of the antibodies (i.e., BsAbs and parent mAbs) and RBD protein were determined by BLI using ForteBIO[®] Octet Qk^e system (FB-40317, PALL). IgGs were captured by anti-human IgG Fc capture (AHC) sensor exposure to SARS-CoV-2 RBD protein in solution to perform the dynamic process of association (200 s) and dissociation (220 s). The experimental data were recorded and analyzed by ForteBIO data analysis software 7.0 (Pall ForteBIO Corporation).

2.6 | Analysis of the blocking activity of antibodies against ACE2 binding to RBD

A competitive binding assay was performed using the ForteBIO[®] Octet Qk^e system (FB-40317, PALL) to verify whether the antibody blocked the binding between RBD and ACE2. Purified ACE2 (HIS tag) at 400 nM from HBS-EP buffer (Cytiva) was loaded onto a single biosensor (HIS 1KB) and washed in HBS-EP buffer for 1 min. After that, 200 nM RBD-FC or RBD-FC was combined with Ab in the sample plate for approximately 10 min. The results were analyzed using Data Analysis Software 7.0 (Pall ForteBIO Corporation).

2.7 | Antibody stability and purity testing

The BsAbs were detected by the T_m (protein melting temperature) and Tagg (protein aggregation temperature) with optional DLS program. The protein particle size distribution and thermal stability were analyzed from multiple angles via the analysis result parameters T_m and Tagg. To test the functional stability of the BsAbs in PBS at different pH values, purified BsAb was diluted in PBS at pH 3.0, 4.0, 5.5, 7.7, and 8.0, and incubated at 37°C for 3 or 21 days. ELISA was used to detect whether the antibody molecules could still efficiently recognize the RBD antigen. To detect BsAb purity, non-reduced capillary electrophoresis (CE-SDS) was performed to determine whether the sample contained foreign bodies, then we performed multi-angle analysis of protein molecular weight heterogeneity via the analysis result parameters RMT (relative migration time), height (peak height), area (peak area), %area (peak area percentage), width (peak width), S/N (signal-to-noise ratio), and resolution rate (resolution).

2.8 | Authentic virus neutralization test

Vero E6 cells were seeded on 96-well culture plates (20 000 cells per well) with DMEM (Gibco) supplemented with 10% FBS, and cultured overnight at 37°C. The antibodies were serially diluted and then mixed with 100 TCID₅₀ (median tissue culture infective dose) SARS-CoV-2. The antibody-virus mixture was added to the plates and incubated at 37°C for 1 h. Then, the supernatant was discarded, DMEM was added to the plate (200 μL per well), and the plate was incubated at 37°C for 72 h. The cells were stained with crystal violet and the absorbance at 570 nm/630 nm was measured. Cells without the antibody-virus mixture were used as the blank control; cells without antibodies were used as the virus controls. The inhibition rate was calculated as (sample signals - virus control signals)/(blank control signals - virus control signals) × 100%. Data were fitted using a 3-parameter logistic model in GraphPad Prism 8.

2.9 | CryoEM grid preparation and data acquisition

A total of 45.55 μL purified wild-type S protein at the concentration of 1.89 mg/mL was incubated with 54.45 μL BI31 at the concentration of 2.5 mg/mL at a 1:2 molar ratio on ice for 40 min for the next step of size exclusion chromatography (SEC). After centrifugation (16 200g, 4°C for 5 min), 100 μL supernatant was injected to GE micro Akta using Superose 6 column. The peak fraction was applied for cryo-EM grid preparation.

An aliquot of 4 μL protein sample of wild-type S-BI31 complex was applied onto a glow-discharged 400 mesh grid (Quantifoil Au R1.2/1.3) supported with a thin layer of GO (Graphene Oxide) and a glow-discharged 400 mesh grid (Quantifoil Au R1.2/1.3) supported with a thin layer of RGO (Reduced Graphene Oxide), blotted with filter paper for 3.0 s and plunge-frozen in liquid ethane using a Thermo Fisher Vitrobot Mark IV. Cryo-EM micrographs were collected on a 300 kV Thermo Fisher Krios G4 electron microscope equipped with a Falcon 4 direct detection camera. The micrographs were collected at a calibrated magnification of $\times 96\,000$, yielding a pixel size of 0.86 Å at a counting mode. In total, the 3119 micrographs (GO) and 357 micrographs (RGO) were collected at an accumulated electron dose of $49.23\text{e}^- \text{Å}^{-2} \text{s}^{-1}$ on each micrograph that was fractionated into a stack of 32 frames with a defocus range of -1.0 to -2.0 μm .

2.10 | EM data processing

Beam-induced motion correction was performed on the stack of frames using MotionCorr2.²⁷ The contrast transfer function (CTF) parameters were determined by CTFFIND4.²⁸ A total of 3515 good micrographs were selected for further data processing using cryoSPARC.²⁹ Particles were auto-picked by the Auto-picking program in cryoSPARC, followed by three rounds of reference-free two-dimensional (2D) classifications. Next, 80 143 particles were selected from good 2D classes and were subjected to two rounds of three-dimensional (3D) classification using a reconstruction of the wild-type S-BI31 complex as a starting model. Four converged 3D classes with a feature containing one wild-type S-BI31 were selected for a final round of 3D refinement. In the three 3D classes, 42 970 particles from one 3D class showing the highest resolution feature with an additional density were selected for 3D refinement, yielding a final reconstruction at a global resolution of 3.50 Å based on the gold-standard Fourier shell correlation criterion at FSC = 0.143. The local resolution was then calculated on the final density map.

The local resolution of the binding region between RBD and BI31 is poor, which is likely due to the flexibility around this region. Local refinement was performed using a mask that retained the binding part of RBD and BI31, yielding a final reconstruction at a global resolution of 3.98 Å based on the gold-standard Fourier shell correlation criterion at FSC = 0.143.

2.11 | Model building and refinement

The model of wild-type S-BI31 complex was built by fitting the model of structure of S-BI31 (predicted by AlphaFold2) into the density map using UCSF Chimera,³⁰ followed by a manual model building in COOT³¹ and a real space refinement in PHENIX.³² The model statistics are listed in Table S1.

2.12 | Protein-protein docking

The protein structures were prepared using UCSF Chimera³⁰ by adding hydrogen atoms and adding AMBER14SB charges to standard residues. H++³³ tool was used to compute pK values of ionizable groups in all protein and adds missing hydrogen atoms according to the specified pH (7.4) of the environment. Then, proteins were subjected to HDock web³⁴ for protein-protein docking. The docking scores are calculated by knowledge-based iterative scoring function ITCPP. A docking score-dependent confidence score was defined to indicate the binding likeliness of two molecules. A more negative docking score means a more possible binding model. The confidence score is above 0.7, the two molecules would be very likely to bind; when the confidence score is between 0.5 and 0.7, the two molecules would be possible to bind; when the confidence score is below 0.5, the two molecules would be unlikely to bind. The open-source software PyMOL 2.0 was used to generate all 3D plots and the academic version Maestro was used to statistics the interaction details.

2.12.1 | Statistical analysis

All experiments were repeated for two or three times with three duplicates, except for the authentic virus neutralization test. Data are presented as the means \pm SD. Statistical significance was determined using GraphPad Prism 8.0 software. The affinity graph was performed, and the EC₅₀ was determined using GraphPad Prism 8.0 software.

3 | RESULTS

3.1 | BsAb construction and purification

BsAb BI31 was composed of SFC3 and HSA-1F, and it was designed as Figure 1A. The SFC3 scFv (VH-linker-VL) was cloned into the N-terminus of the HSA-1F antibody VH. The plasmids with light and heavy chains of the modified antibodies were co-transfected into FreeStyle™ 293-F cells. After 72 h, the antibody was purified and analyzed by 10% SDS-PAGE under nonreducing and reducing conditions. Figure 1B shows the size of the antibody. Compared

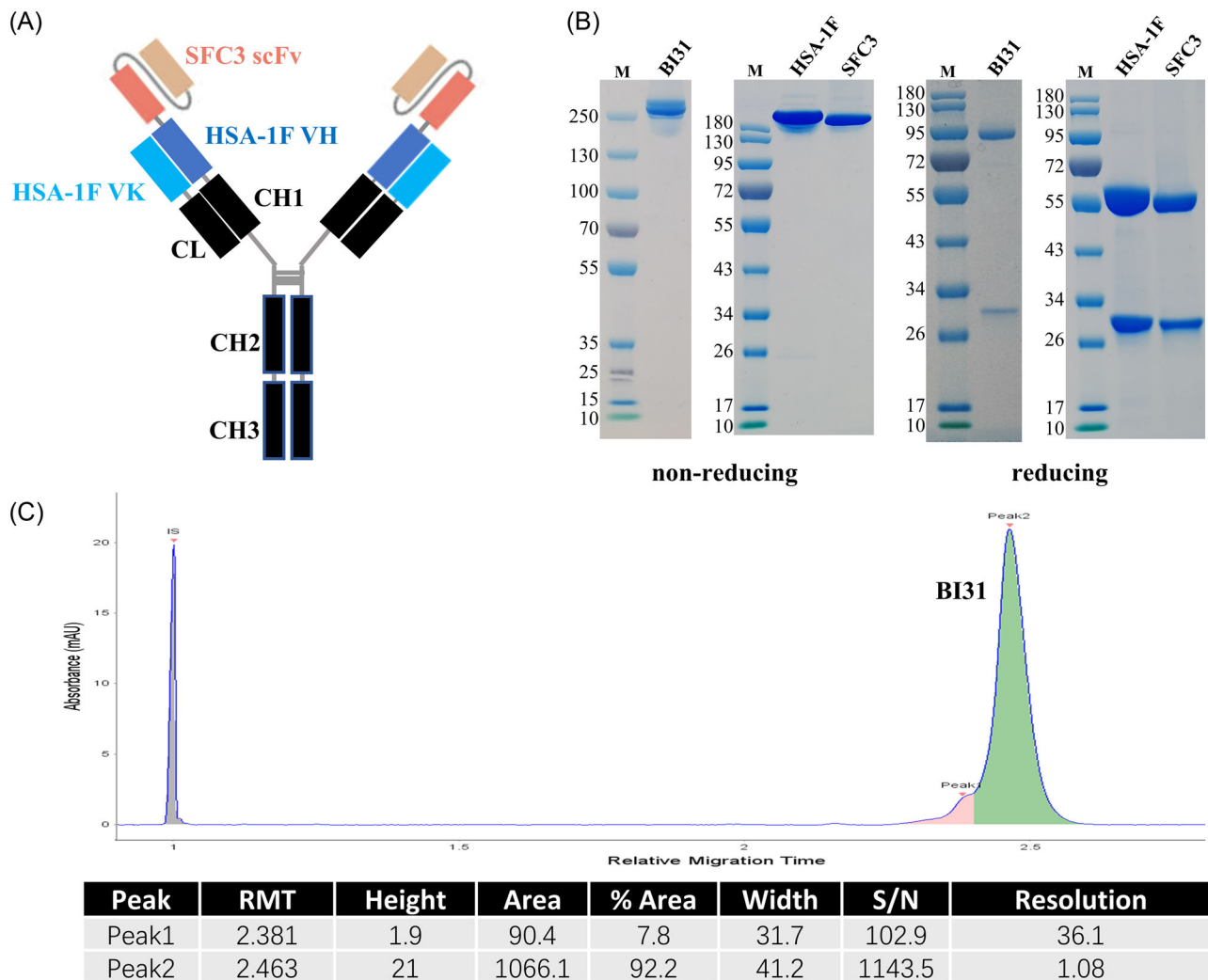


FIGURE 1 Structural characterization and identification of BI31. (A) Schematic of the structure of BI31. (B) The purified antibodies were analyzed by sodium dodecyl sulfate-polyacrylamide gel electrophoresis under nonreducing (left) and reducing (right) conditions. The heavy chain (HC) and light chain (LC) of each antibody were of the expected size. (C) The results of CE-SDS of BI31. The leftmost peak is the marker control, and the peak on the right (green, Peak 2) is the sample peak.

with the parent antibody, the increased size of the heavy chain was reflective of the additional scFv on each chain and was consistent with the molecular weights. CE-SDS showed that the bispecific antibody BI31 had a small amount of aggregation, with 92% purity (Figure 1C).

3.2 | Bispecific antibody binding activity

ELISA was performed to test the affinity of the BsAbs and the parent antibody to the SARS-CoV-2 RBD protein. Both the BsAbs and parent antibody could bind specifically to the SARS-CoV-2 S protein RBD (Figure 2A). The BsAbs had a similar affinity to the parent antibody for the RBD, and the EC_{50} was about 0.01 nM (Table 1). The affinity test of the antibodies to several SARS-CoV-2 variants RBD was also performed (Figure 2B-G, the EC_{50} was shown in Table 1). As shown in Figure 2B-D, the affinity of the

BsAbs to Alpha (B.1.1.7), Beta (B.1.351), Gamma (P.1) was near the SARS-CoV-2 (Wuhan-Hu-1) RBD, and higher than SFC3. The affinity of the BsAbs to Delta (B.1.617.2) decreased; the reason might be the decreased affinity of HAS-1F to Delta (B.1.617.2) (Figure 2E). To the latest variants Omicron (B.1.1.529) and Omicron (XBB), the affinity of the BsAbs reached to 0.21 and 0.38 nM, even the parent antibody had weak binding ability to Omicron (XBB) RBD (Figure 2F,G and Table 1).

Considering that SARS-CoV, MERS-CoV, and SARS-CoV-2 all belong to coronavirus subgenus β and their RBD region has certain homology, we tested the affinity of the parent antibody and BI31 to RBD of SARS-CoV and MERS-CoV, respectively. The parent antibody had weak binding ability to the SARS-CoV and MERS-CoV RBD proteins, whereas BI31 had significantly improved affinity for them (Figure 2H,I). We speculate that the unique dual binding site of the BsAb enables its more effective binding to the SARS-CoV and MERS-CoV RBDs, achieving the effect of $1 + 1 > 2$.

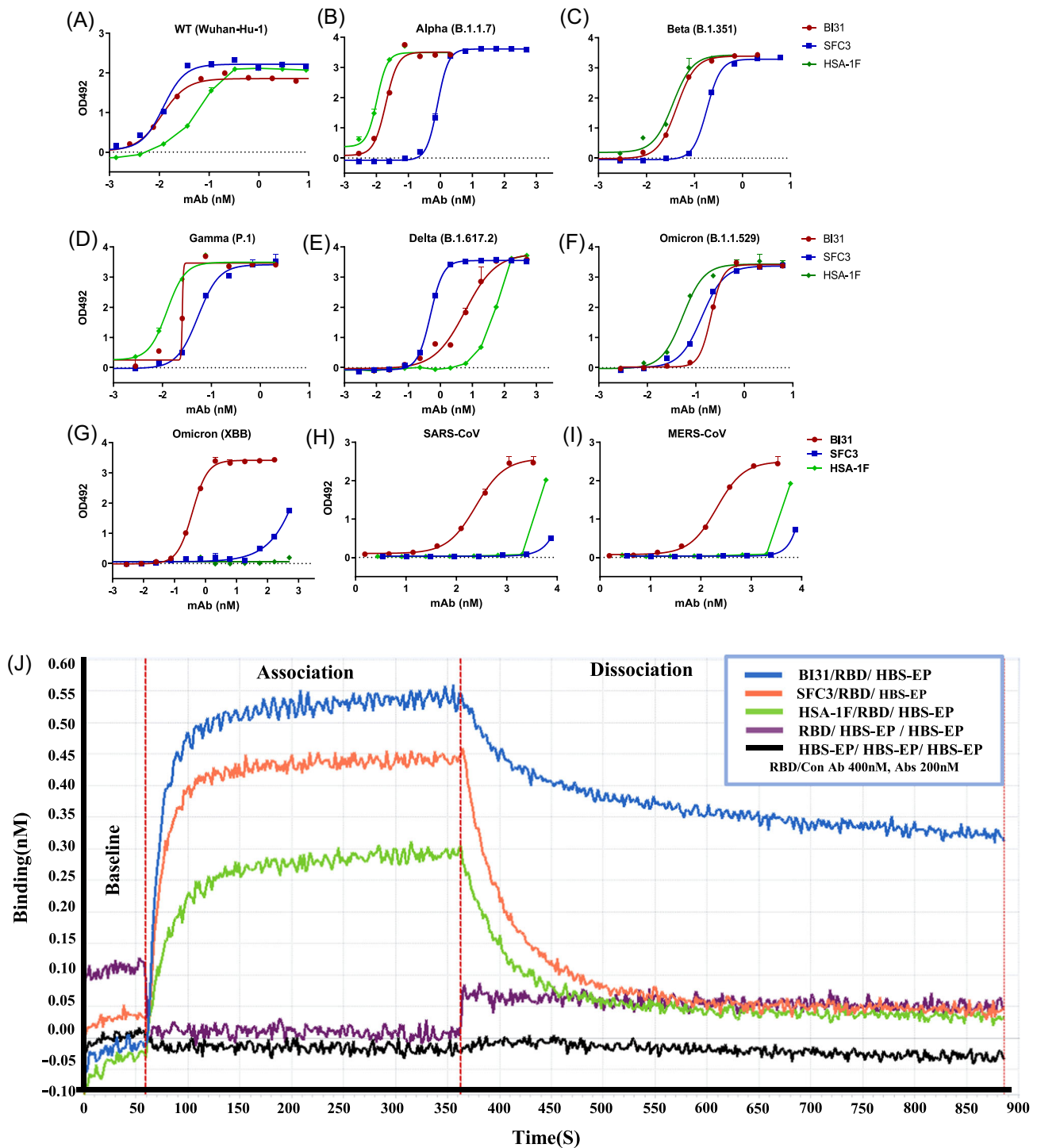


FIGURE 2 BI31 shows better binding ability to the SARS-CoV-2, SARS-CoV, and MERS-CoV S RBDs than the parental mAbs. (A–F) ELISA detection of BsAb, SFC3, and HSA-1F binding to the S RBDs of (A) SARS-CoV-2, (B) mutant strain of SARS-CoV-2 B.1.617.1, (C) mutant strain of SARS-CoV-2 B.1.617.2, (D) mutant strain of SARS-CoV-2 N501Y.V2, (E) SARS-CoV, and (F) MERS-CoV. The data represent the average and standard deviation of three independent variables. The EC_{50} value was obtained via nonlinear regression. (G) The binding kinetics of BI31 to the SARS-CoV-2 S1 RBD. In the legend box, the samples were separated by slash (/), respectively, to represent “loading”, “association”, and dissociation stages of sample molecules.

To test their binding activity, we examined the parent mAb and BsAb binding to the SARS-CoV-2 RBD in an Octet-based binding assay (Figure 2J). The BsAb had a significantly higher binding curve than the parent antibodies, which is consistent with the size of each

molecule. BI31 showed strong monovalent binding to RBD. Compared with BI31, SFC3 and HSA-1F had faster disassociation profiles. THC antigen was used as the negative control to confirm the specific association between the test antibodies and the RBD. BI31 showed

TABLE 1 Antibody affinity analysis.

RBD	EC ₅₀ (nM)		
	BI31	SFC3	HSA-1F
SARS-CoV-2 (Wuhan-Wu-1)	0.01	0.02	0.05
SARS-CoV-2 (Alpha B.1.1.7)	0.02	0.81	0.01
SARS-CoV-2 (Beta B.1.351)	0.04	0.18	0.04
SARS-CoV-2 (Gamma P.1)	0.03	0.05	0.01
SARS-CoV-2 (Delta B.1.617.2)	5.93	0.49	49.48
SARS-CoV-2 (Omicron B.1.1.529)	0.21	0.13	0.05
SARS-CoV-2 (Omicron XBB)	0.38	-	-
SARS-CoV	244.8	-	-
MERS-CoV	206.7	-	-

stronger binding affinity in the RBD association and disassociation experiment, which means that the BsAbs have potential for longer-lasting protection against SARS-CoV-2.

3.3 | BI31 is a potential broad-spectrum antibody against Betacoronavirus

The neutralizing ability of BI31 was first tested using the SARS-CoV-2 S pseudovirus (HIV vector with luciferase reporter gene). The parent antibodies and their combination were also assessed. BI31 and the parent antibodies could fully neutralize the S pseudovirus, as they all blocked the infection of S pseudovirus to Huh7 cells expressing ACE2 (Figure 3A). When SFC3 and HSA-1F were used alone or combined, the EC₅₀ of blocking S pseudovirus was 0.70, 5.80, and 4.10 nM, respectively, and the EC₅₀ of BI31 was lower to 0.5 nM (Table 2).

Compared with the original strain, several studies have shown that the SARS-CoV-2 variants were often more infectious.⁵ To further test the neutralizing activity, we performed neutralization assays again with the BsAbs and the combination of mAbs using the common SARS-CoV-2 variant pseudotype, such as Alpha (B.1.1.7), Beta (B.1.351), Gamma (P.1), Delta (B.1.617.2), and Omicron (B.1.1.529, BF.7, XBB). As shown in Figure 3B–H and Table 2, neutralizing activity was exhibited on BI31 and its parental antibodies. First, the parental mAb and the combination of mAbs were observed to have good neutralizing effects to Alpha (B.1.1.7), Beta (B.1.351), Gamma (P.1), Delta (B.1.617.2), and Omicron (B.1.1.529); however, the neutralizing activity of BI31 was lower on Alpha (B.1.1.7) and not detected on Delta (B.1.617.2). Fortunately, BI31 has a strong neutralizing activity against Omicron (B.1.1.529) with an EC₅₀ of 0.01 nM, which far exceeds the effect of the parental antibody. Besides, when the parental mAb and the combination of mAbs had no neutralizing effects to Omicron (BF.7, XBB), the neutralizing activity of BI31 was detected with EC₅₀ of 16.4 and 15.8 nM. In general, BI31 has neutralizing activity against various

COVID-19 variants, which is important in response to viral immune escape.

Then three reported sites (D614G,³⁵ N501Y,³⁶ E484K³⁷) that can significantly enhance viral infectivity were selected for neutralization activity experiments. After neutralization experiment, the loss of neutralizing activity of the tested antibodies was not observed, which indicated that it may have good neutralizing activity against D614G and N501Y variants (Figure S1). However, the neutralizing activity of the BI31 against the E484K variants was significantly reduced. We speculate that the 484 site is likely to be the key site for the neutralizing effect of the BI31.

Considering that both mAbs and BI31 could bind to the SARS-CoV and MERS-CoV RBDs, we tested the neutralizing activity of the BsAb against SARS-CoV and MERS-CoV S pseudovirus in Huh7 cells (Figure 3I,J). We were surprised to find that BI31 had neutralizing activity against both, while the parental antibody cocktail had no neutralizing effect. The reciprocal EC₅₀ neutralization titers of BI31 against SARS-CoV and MERS-CoV pseudovirus were 7.80 and 5.30 nM, respectively. This means that BI31 is expected to become a broad-spectrum antibody against coronavirus even if the effective antibody concentration against the other coronavirus had been diluted compared with the SARS-CoV-2.

We next performed in vitro neutralization experiments using authentic SARS-CoV-2. Vero E6 cells containing authentic SARS-CoV-2 were neutralized by BI31 with an EC₅₀ of 3 nM (Figure 3K). The BsAb was superior to its parental antibody SFC3, which had an EC₅₀ of 5.4 nM, and was inferior a little to that of the parental combination, which had an EC₅₀ of 1.23 nM. HSA-1F could not completely protect the Vero E6 cells against authentic SARS-CoV-2 infection, so the conditions did not permit the calculation of the EC₅₀. Unfortunately, we were unable to detect in vitro neutralization experiments using authentic SARS-CoV and MERS-CoV limited by the experimental conditions.

3.4 | Antibody blocking activity assay

To further explore the mechanism of antibody neutralization, competitive binding experiments were performed by ForteBIO. First, the antibody FC domain is connected to the RBD molecule of the SARS-CoV-2, which can not only reflect the experimental results more clearly but also exclude the possible steric hindrance of the antibody Fc. As shown in Figure 4, the binding values of the mixture of antibody and RBD-Fc were not observed to increase significantly. In contrast, the binding values of the single RBD-Fc or the mixture of Con Ab and RBD-Fc increased significantly. This indicates that the neutralization against the SARS-CoV-2 from the BsAb and parental antibody is carried out by blocking the binding of RBD to ACE2.

In addition, we performed the same competition experiments for the RBD of SARS-CoV and MERS-CoV, respectively, by ForteBIO. However, similar results were not obtained. Antibody (BsAb or mAbs) could not block the binding of the RBD of SARS-CoV and MERS-CoV to the corresponding functional receptors (ACE2 or DPP4). We

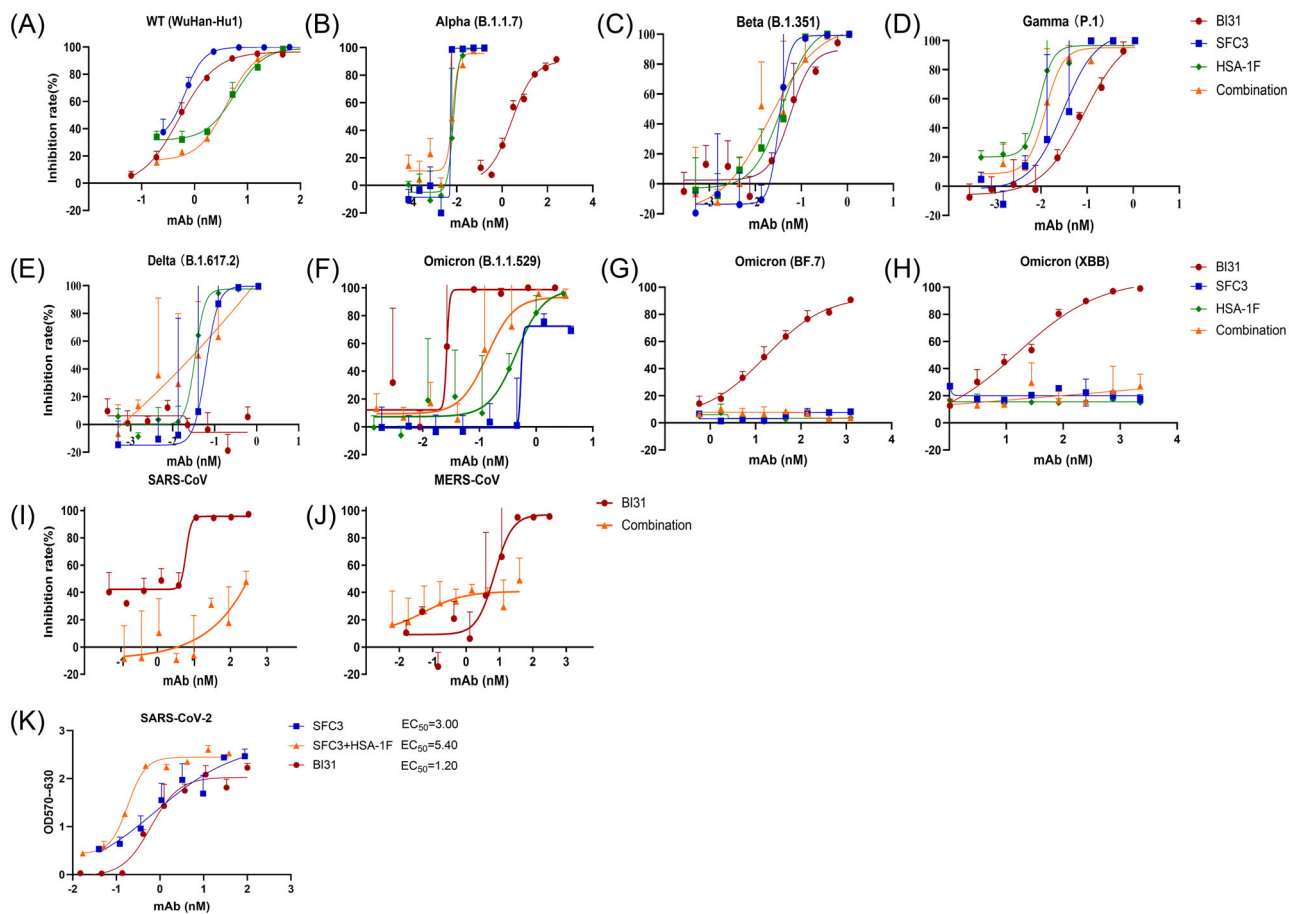


FIGURE 3 BI31 is more effective than the parental mAbs in neutralizing SARS-CoV-2 and has a broad anti-coronavirus spectrum. (A–I) Pseudovirus neutralization curves of BI31 SFC3, HSA-1F, and parental antibody combination(1:1 ratio) for: (A) SARS-CoV-2 S pseudovirus, (B) SARS-CoV-2 Alpha variant (B.1.1.7) pseudovirus, (C) SARS-CoV-2 Beta variant (501Y.V2) pseudovirus, (D) SARS-CoV-2 Gamma variant (P.1) pseudovirus, (E) SARS-CoV-2 S Delta variant (B.1.617.2) pseudovirus, (F) SARS-CoV-2 S Omicron variant (B.1.1.529) pseudovirus, (G) SARS-CoV-2 S pseudovirus, and (H) MERS-CoV S pseudovirus. (I) Authentic SARS-CoV-2 neutralization (1:1 ratio) curves of BI31, SFC3, HSA-1F, and the SFC3 and HSA-1F combination; HSA-1F did not show neutralizing activity. The data represent the average and SD of two independent variables. The EC₅₀ value was obtained via nonlinear regression. The value of EC₅₀ was the total antibody concentration.

speculated that BI31 had a lower affinity to SARS and MERS RBD than the receptors.

3.5 | Structural analysis of BI31:Spike complex

To understand the mechanism of the neutralizing activity of BI31 against the SARS-CoV-2, we determined the cryo-EM structure of BI31 bound to the spike protein ectodomain trimer of the Wuhan-hu-1 strain SARS-CoV-2 (Figure S2 and Table S1). With local refinement, we obtained the cryo-EM structure at an overall 3.98 Å resolution, which allowed us to reveal the detailed binding interface (Figure S3). There were two Fabs and one scFv of BI31 involving the complex. Two Fabs of BI31 bound to the standing-up state RBD of spike trimer *in vitro*, and one scFv of BI31 bound to the lying-down state RBD of spike trimer (Figure 5A,B). The RBD in coronaviruses can be in either a standing-up state, which enables receptor binding, or a lying-down state, which does not bind to the host receptors, but contributes to the immune evasion

of SARS-CoV-2 as one of the conformational masking strategies.³⁸ The RBD constantly switches between the standing-up state and the lying-down state. For BI31 can bind to both standing-up and lying-down state RBDs, it might be much easier to capture SARS-CoV-2.

Furthermore, the detailed binding interface was revealed to show in Figure 5C–I, five chains of BI31 all recognized a region of the RBD from aa 470 to 500. The heavy and light chain binding to monomer A of Spike trimer formed a Fab, as the other couple binding to monomer B. Though the sequences of two Fabs were the same, the binding format was different. In the Fab binding to monomer A, the heavy chain had much more binding interfaces; however, in the Fab binding to monomer B, so did the light chain. The scFv fused to one heavy chain of the two Fabs, but it failed to resolve the fusion. According to the structure, we speculated the scFv fused to the heavy chain binding to monomer A of Spike trimer. With the help of scFv binding to the lying-down state Spike, it might be the reason that there were more amino acid residues of the heavy chain involving the binding interfaces.

We mapped this region of the RBD, including the original Wuhan-hu-1 strain, Alpha strain, Beta strain, Omicron strain, and so on (Figure S4). There were four mutations from aa 470 to 500 of the RBD, S477N, T478K, E484Q/K/A, and F486V/S. S477, and E484 were both involved in one chain interaction. T478 and F486 were involved in four and three chains interaction, so these two mutations would interfere the binding of BI31. However, considering the five

chains of BI31 bind to this region to form over 30 hydrogen bonds, several mutations would only decrease the interaction a little.

To explore the interaction between BI31 and RBD of SARS-CoV and MERS-CoV, five kinds of S trimers conformations from the Protein Data Bank were analyzed for docking with cryo-EM structure of BI31. The docking structures are shown in Figure S5-S10. The docking scores are listed in Table S2. Cryo-EM structure of the BI31:SARS-CoV-2 Spike complex had the highest docking score, and MERS-CoV S conformation 1 (PDB codes: 5X5C) and SARS-CoV S conformation 2 (PDB codes: 5X5B) were a little lower. 5X5C and SARS-CoV-2 had a similar structure with two RBDs in standing-up state and one RBD in lying-down state, while 5X5B had one RBD in standing-up state and two RBDs in lying-down state. The other three conformations had much lower docking scores (5X5F of MERS-CoV with one RBD in standing-up state, 7V3L of MERS-CoV with three RBDs in standing-up state, and 5x58 of SARS-CoV with three RBDs in lying-down state). These indicated BI31 preferred to bind S trimers conformations with two RBDs in standing-up state and one RBD in lying-down state.

TABLE 2 Antibody neutralization activity analysis.

Pseudovirus	EC ₅₀ (nM)			
	BI31	SFC3	HSA-1F	Combination
SARS-CoV-2 (Wuhan-Wu-1)	0.50	0.70	5.80	4.10
SARS-CoV-2 (Alpha B.1.1.7)	13.16	0.03	0.04	0.04
SARS-CoV-2 (Beta B.1.351)	0.05	0.03	0.04	0.02
SARS-CoV-2 (Gamma P.1)	0.08	0.03	0.01	0.01
SARS-CoV-2 (Delta B.1.617.2)	-	0.06	0.03	0.05
SARS-CoV-2 (Omicron B.1.1.529)	0.01	0.50	0.40	0.10
SARS-CoV-2 (Omicron BF.7)	16.4	-	-	-
SARS-CoV-2 (Omicron XBB)	15.8	-	-	-
SARS-CoV	7.80	-	-	-
MERS-CoV	5.30	-	-	-

3.6 | Analysis of BsAb structural and functional stability in vitro

The physicochemical properties of BsAb were evaluated with optional Tm and Tagg with optional DLS. The purpose was to determine whether it is suitable for large-scale production, which is essential for commercial antibody development. The Tm1 and Tagg of BI31 were 43.4°C and 44.3°C (Figure 6A and Table S3). In addition, a

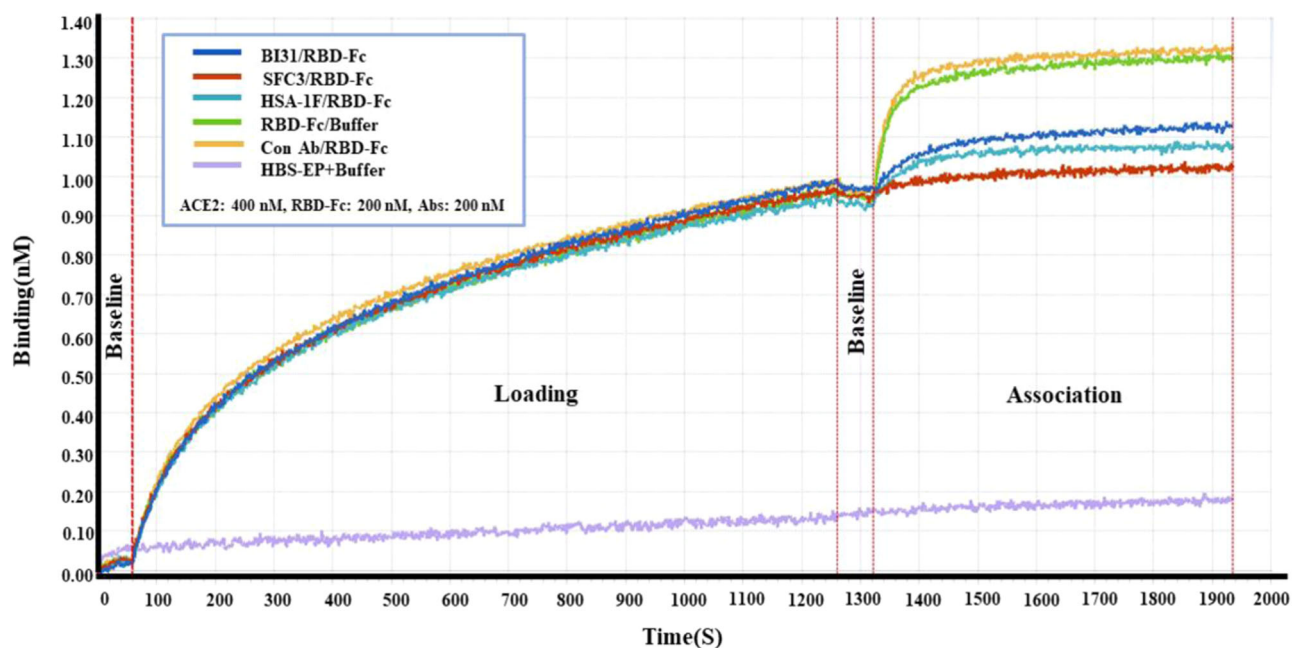


FIGURE 4 Antibody blocking activity assay. Both BsAb BI31 and parental antibodies can effectively block the binding of SARS-CoV-2 RBD to ACE2. In the legend box, the samples separated by slash (/), respectively, represent “loading” and “association” stages of sample molecules. The experiment was performed in two independent repetitions with consistent results.

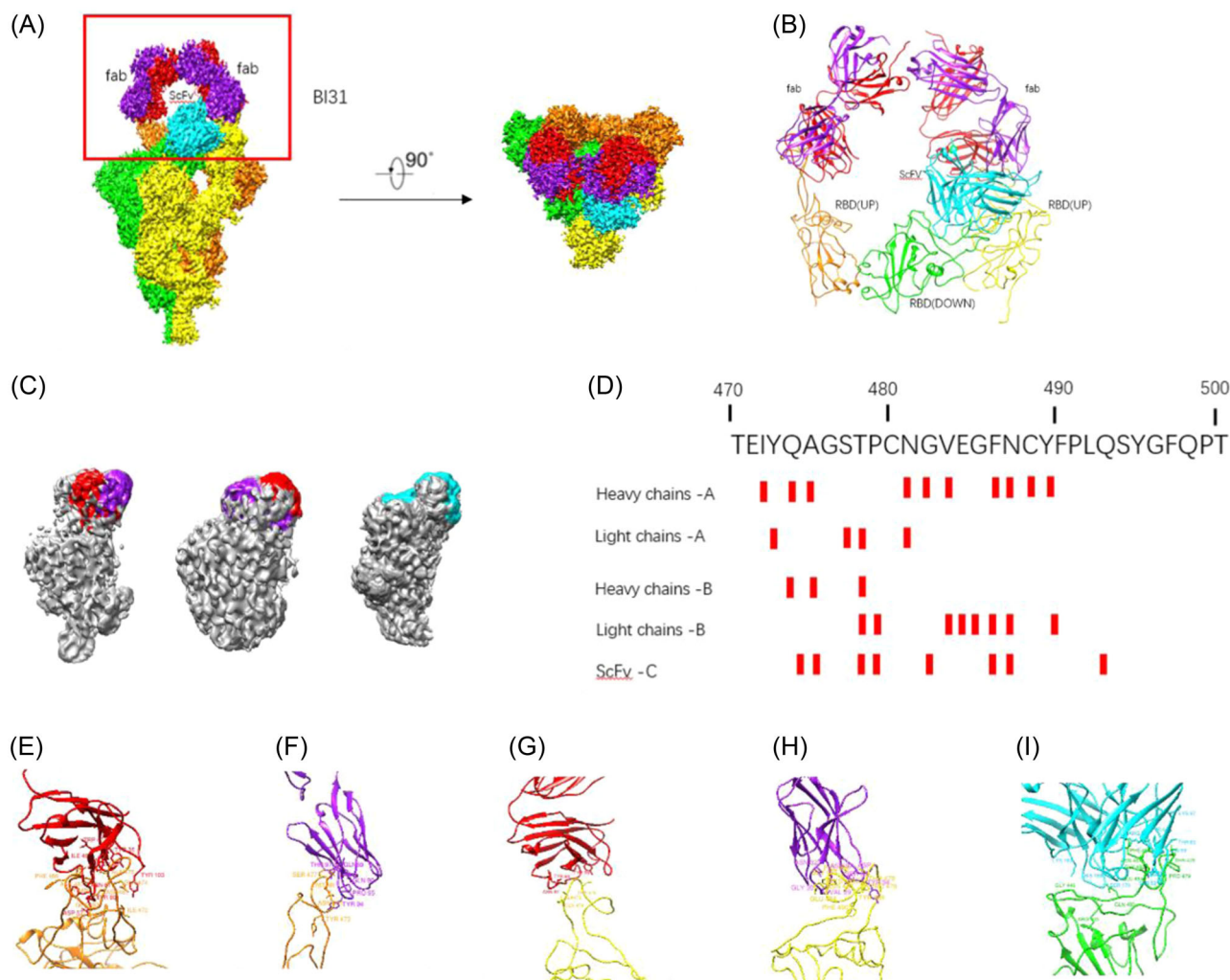


FIGURE 5 Cryo-EM structure and analysis of BI31 and the complex with SARS-CoV-2 S protein. (A, B) The domain-colored cryo-EM map of SARS-CoV-2 S ectodomain trimer and BI31 fragments complex is shown, viewed along two perpendicular orientations. (C) The epitope surfaces of S-chain A bind with BI31 (left), S-chain B with BI31 (mid), and S-chain C with BI31 (right). Heavy chains (red), light chains (purple), and scFv (blue). (D) BI31 positioning on SARS-CoV-2. (E–I), The details of S-chain A (orange) bind with BI31 heavy chain (E) and light chain (F), of S-chain B (yellow) bind with BI31 heavy chain (G) and light chain (H). S-chain C (I) binds with scFv (blue).

slight aggregation was detected in BI31 through further analysis of mass and light intensity (Figure S11). The Peak1 (target Peak) mass ratio of the sample obtained by calculation is 94.68% (Table S4), which indicates that the degree of aggregation is not large and can be optimized through subsequent optimization. Considering its unique structural complexity, its thermal stability and degree of polymerization performance were in line with expectations, and there was no obvious abnormality.

To test the functional stability of the antibodies at different pH values, we incubated them at 37°C at pH 3, 4, 5.5, and 8 in PBS for 3, 7, 14, and 21 days, and then used ELISA to detect their ability to bind to the RBD. The original sample stored at 4°C (pH 7.2) and the original sample incubated at 37°C (pH 7.2) as controls were also tested at the same time. Compared with the original sample, BI31 was stable in neutral and acidic environments, and the sample incubated for 21 days retained the same binding activity as that

before incubation (Figure 6B–E). Alkaline conditions had a greater impact on the BsAb. On Day 3, the binding activity of BI31 had decreased significantly. On Day 7, it had completely lost its affinity for the SARS-CoV-2 S-RBD. These results show that BI31 can fully adapt to neutral environment and acidic environments and further demonstrate its reliability at physiological pH.

4 | DISCUSSION

BsAbs are new types of antibody in addition to mAbs and antibody combination therapy. They can bind to ≥ 2 antigen-binding epitopes simultaneously,³⁹ which means that the bivalent antibody retains the advantages of the antibody cocktail in the form of a single molecule.²⁴ This can increase therapeutic efficacy and prevent viral evasion.

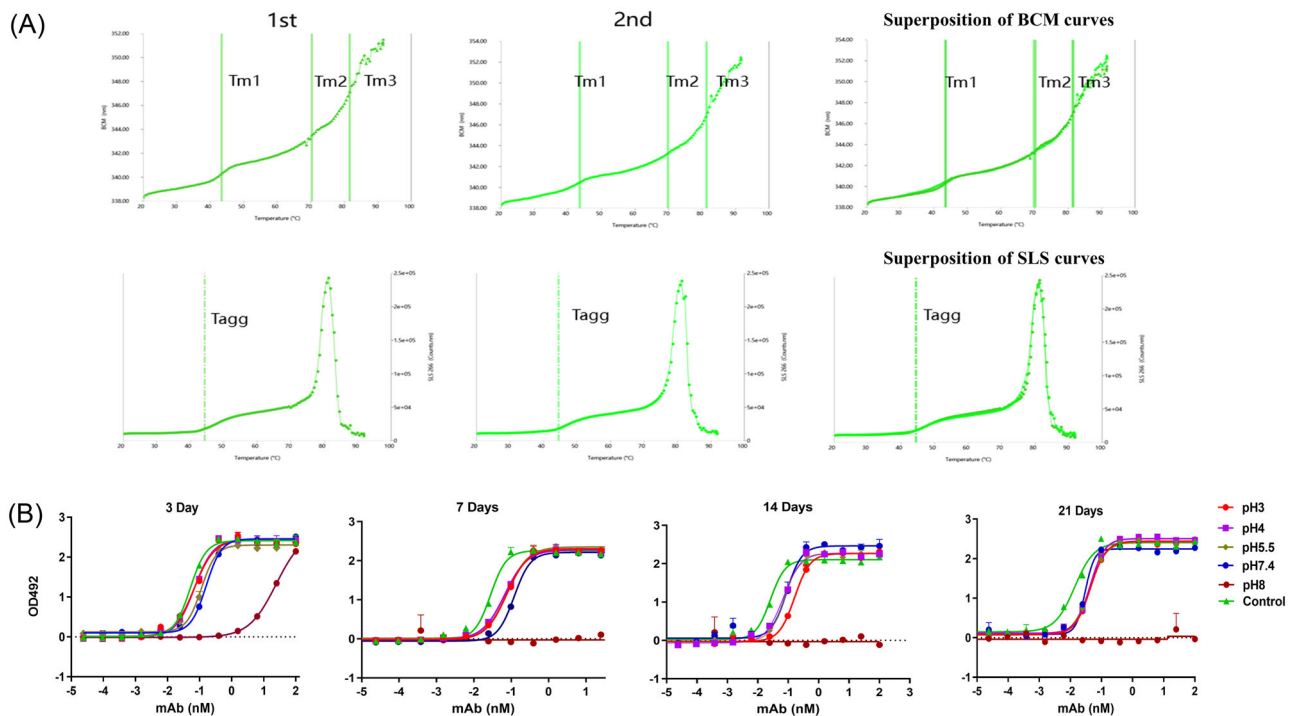


FIGURE 6 Structural stability and functional stability analysis of BI31. (A) Tm and Tagg with optional DLS detection of the development characteristics of the chemical properties of BI31. The data come from two independent replicate experiments. (B–E) ELISA of BI31 and SARS-CoV-2 S1 RBD binding in phosphate-buffered saline (PBS). The purified BI31 was diluted with PBS at pH 3, 4, 5.5, and 8 and then incubated at 37°C for 3 days (B), 7 days (C), 14 days (D), and 21 days (E). The control was the 4°C sample without pH adjustment after purification. The EC₅₀ value was obtained via nonlinear regression. The data represent the average and SD of two independent variables.

Here, based on previous research, we constructed a novel IgG-like BsAb, BI31, with two synergistic neutralizing mAbs targeting SARS-CoV-2 S RBD. As purifying and preparing BsAbs is a known difficulty,⁴⁰ we chose a symmetrical structure to connect the scFv of SFC3 to the N-terminus of the heavy chain of HSA-1F, which can minimize the mismatch of the light and heavy chains and reduces the difficulty of BsAb preparation and purification.^{41,42} Several fusion formats were chosen to connect the scFv and the heavy chain, the results showed the rigid connection format without linker (BI31) had the best neutralization effect. That might be because the scFv bound to the lying-down RBD, the rigid connection format pulled the heavy chain to further bind with the standing-up state RBD.

The detailed binding interface showed five chains of BI31, all recognized a region of the RBD from aa 470 to 500 which was also the epitope of hACE2. There were eight amino acid residues binding to hACE2, including A475, F486, N487, Y489, Q493, G496, Q498, and T500.⁴³ Among them, five amino acid residues bound to BI31 too, A475, F486, N487, Y489, and Q493. Thus, BI31 was able to block the binding between RBD and hACE2. These were consistent with experimental results (Figure 4). However, there were also some inconsistencies which confused us. The pseudovirus neutralization results of variants (Figure 3) were not totally consistent with the sequence alignment (Figure S4). Even Alpha variant had no mutation from aa 470 to 500; the neutralizing activity of BI31 was much lower on Alpha (B.1.1.7) than on Beta (501Y.V2) and Gamma (P.1) which

had one significant mutation E484K. The Delta variant had one mutation T478K from aa 470 to 500, and the neutralizing activity of BI31 was not detected on Delta (B.1.617.2). These all indicated that in addition to the revealed binding interface, there might be other regions that affect the neutralization activity of BI31. Second, in the preliminary work of competitive binding assay, even when the binding between SFC3 and RBD reached saturation, HSA-1F still combine with RBD to increase the signal, and vice versa.²⁶ These results revealed that SFC3 and HSA-1F did not bind to RBD competitively, we speculated the two mAbs recognize different RBD epitopes. However, scFv of SFC3 and Fab of HSA-1F recognized an identical region of the RBD from aa 470 to 500. That might be due to the fusion expression of scFv and Fab, the rigid connection format without linker influenced the respective epitopes. This conflict could only be explained by resolving the respective structures of mAbs and Spike trimer.

In the past 3 years, many SARS-CoV-2 neutralizing antibodies (NABs) were developed with efficient therapeutic potential to deal with the rapid emergence of COVID-19.^{44–48} Huang et al. provided a systemic overview of categorizing SARS-CoV-2 specific or cross-reactive Nabs into four types (Type-I to Type-IV) pursuant to the conformations of bound RBD on S trimer and therefore lead to four distinct conformations of S trimers (All “down” RBDs; one “up” RBD; two “up” RBDs and three “up” RBDs).⁴⁹ Interestingly, those NABs that appear in the same type seem to prevent the viral infection with a

similar mechanism. In the preliminary work, we performed competitive binding between CB6, REGN10933, P2B-2F, REGN10987, S2A4, and MW05 with SFC3 and HSA-1F.²⁶ CB6, REGN10933, P2B-2F, REGN10987 were mentioned in the review article. SFC3 had competition with CB6 (Type-I), REGN10933 (Type-I), P2B-2F (Type-IV), and REGN10987 (Type-IV). HSA-1F had competition with CB6 (Type-I), REGN10933 (Type-I). The NAb in Type-I can only bind to the “up” RBD, besides epitopes of Type-I NAb are extensively overlapping with the binding site of hACE2.⁴⁹ For the overlapping epitopes, SFC3 and HSA-1F both had competition with CB6 (Type-I), REGN10933 (Type-I), though SFC3 bound to the “down” RBD. Type-IV NAb can recognize the epitopes on both the “up” and “down” state of RBDs because they target to two different regions, one is located on the receptor binding motif (RBM) and the other is located on the side of the RBD with no or little overlap with the RBM.⁴⁹ SFC3 had competition with Type-IV NAb P2B-2F and REGN10987, which suggested that mAb SFC3 might bind to “up” RBD also. Besides, REGN10933 and REGN10987 have developed as a therapeutic cocktail. HAS-1F and SFC3 had similar characteristics and synergistic effects with combo using, so they were valuable to develop.

BsAb BI31 was constructed based on SFC3 and HSA-1F which had synergistic neutralizing capacity. Except for neutralizing activity against SARS-CoV-2 and many variants, BI31 had neutralizing activity against SARS-CoV and MERS-CoV, while the parental antibody cocktail had no neutralizing effect. The binding sites of BI31 were not conserved between SARS-CoV, MERS-CoV, and SARS-CoV-2. The cross-binding of BI31 to SARS-CoV and MERS-CoV might differ with binding to SARS-CoV-2. Protein-protein docking was used to explore the interaction between BI31 and S trimers of SARS-CoV and MERS-CoV. In the five conformations, 5X5C of MERS-CoV had a similar structure with SARS-CoV-2 which BI31 bound to, and there were two RBDs in standing-up state and one RBD in lying-down state. The docking score of BI31:5X5C was near the BI31:SARS-CoV-2 Spike complex, which indicated the binding of BI31:5X5C was just lower a little than the BI31:SARS-CoV-2 Spike complex. The second docking score was 5X5B of SARS-CoV, which had one RBD in a standing-up state and two RBDs in a lying-down state. These indicated BI31 might bind multiple S trimers conformations and then have cross-binding activity. Besides, we speculate that the unique spatial advantage of the BsAb enables its cover of the nonbinding sites on the antigen when it binds to the target antigen. The covered sites are likely to play an important role in host cell infection by SARS-CoV and MERS-CoV. These characteristics confer on BI31 the ability to neutralize SARS-CoV and MERS-CoV, which also indicates that it has great potential to be a broad-spectrum antibody against coronavirus.

AUTHOR CONTRIBUTIONS

Conceptualization: Zhixin Yang and Junjie Xu; **funding acquisition:** Junjie Xu and Zhixin Yang; **experiment design:** Rong Wang and Zhixin Yang; **construction, expression, and purification of antibodies:** Rong Wang and Jiazheng Guo; **ELISA for binding activity test:** Lei Chen; **FortéBIO for binding and blocking activity assay:** Peng Du and Jiazheng Guo; **neutralization assay of pseudovirus:** Jiansheng Lu and Rong Wang; **structural and functional**

stability: Rong Wang and Jiazheng Guo; **neutralization assay of authentic virus:** Jun Zhang; **data analysis:** Rong Wang, Zhixin Yang, YunZhou Yu, Jiansheng Lu, and Peng Du; **manuscript writing:** Jiazheng Guo and Rong Wang; **manuscript review & editing:** Zhixin Yang, Junjie Xu, and YunZhou Yu. All authors have read and approved the article.

ACKNOWLEDGMENTS

We thank the Institute of Microbiology and Epidemiology, Academy of Military Medical Sciences, China, for providing the SARS-CoV-2. We thank Prof. Lihua Hou (Beijing Institute of Biotechnology) for kindly providing the plasmid pNL4.3-luc-R⁻E⁻. We thank Prof. Jun Wu and Bo Liu (Beijing Institute of Biotechnology) for kindly providing RBD. We thank Prof. Jiannan Feng (Beijing Institute of Pharmacology and Toxicology) for his insightful comments. This work was supported by the National Key R&D Program of China [2020YFC0841400].

CONFLICT OF INTEREST STATEMENT

Zhixin Yang, Rong Wang, Jiazheng Guo, Jiansheng Lu, Peng Du, Yun Zhou Yu, and Lei Chen are listed as inventors on a pending patent application for BsAb BI31. The remaining authors declare no conflict of interest.

DATA AVAILABILITY STATEMENT

The data supporting the findings of this study can be obtained from the corresponding authors upon reasonable request.

ORCID

Jiazheng Guo  <http://orcid.org/0000-0002-0092-5068>

REFERENCES

- Zhu N, Zhang D, Wang W, et al. A novel coronavirus from patients with pneumonia in China, 2019. *N Engl J Med*. 2020;382(8):727-733.
- Li W, Moore MJ, Vasilieva N, et al. Angiotensin-converting enzyme 2 is a functional receptor for the SARS coronavirus. *Nature*. 2003;426(6965):450-454.
- Chan JFW, Lau SKP, Woo PCY. The emerging novel Middle East respiratory syndrome coronavirus: the “knowns” and “unknowns”. *J Formos Med Assoc*. 2013;112(7):372-381.
- Focosi D, Franchini M. COVID-19 neutralizing antibody-based therapies in humoral immune deficiencies: a narrative review. *Transfus Apher Sci*. 2021;60(3):103071.
- Weisblum Y, Schmidt F, Zhang F, et al. Escape from neutralizing antibodies by SARS-CoV-2 spike protein variants. *eLife*. 2020;9:e61312.
- Letko M, Marzi A, Munster V. Functional assessment of cell entry and receptor usage for SARS-CoV-2 and other lineage B betacoronaviruses. *Nat Microbiol*. 2020;5(4):562-569.
- Li F. Structure, function, and evolution of coronavirus spike proteins. *Annu Rev Virol*. 2016;3(1):237-261.
- Zhou P, Yang XL, Wang XG, et al. A pneumonia outbreak associated with a new coronavirus of probable bat origin. *Nature*. 2020;579(7798):270-273.
- Lai CC, Shih TP, Ko WC, Tang HJ, Hsueh PR. Severe acute respiratory syndrome coronavirus 2 (SARS-CoV-2) and coronavirus disease-2019 (COVID-19): the epidemic and the challenges. *Int J Antimicrob Agents*. 2020;55(3):105924.
- Huang C, Wang Y, Li X, et al. Clinical features of patients infected with 2019 novel coronavirus in Wuhan, China. *Lancet*. 2020;395(10223):497-506.

11. Zhu FC, Li YH, Guan XH, et al. Safety, tolerability, and immunogenicity of a recombinant adenovirus type-5 vectored COVID-19 vaccine: a dose-escalation, open-label, non-randomised, first-in-human trial. *Lancet*. 2020;395(10240):1845-1854.
12. Amanat F, Krammer F. SARS-CoV-2 vaccines: status report. *Immunity*. 2020;52(4):583-589.
13. Li Q, Liu Q, Huang W, et al. An LASV GPC pseudotyped virus based reporter system enables evaluation of vaccines in mice under non-BSL-4 conditions. *Vaccine*. 2017;35(38):5172-5178.
14. Miao X, Luo Y, Huang X, et al. A novel biparatopic hybrid antibody-ACE2 fusion that blocks SARS-CoV-2 infection: implications for therapy. *Mabs*. 2020;12(1):1804241.
15. Wang C, Li W, Drabek D, et al. A human monoclonal antibody blocking SARS-CoV-2 infection. *Nat Commun*. 2020;11(1):2251.
16. Wrapp D, De Vlieger D, Corbett KS, et al. Structural basis for potent neutralization of betacoronaviruses by single-domain Camelid antibodies. *Cell*. 2020;181(5):1004-1015.
17. Yuan M, Wu NC, Zhu X, et al. A highly conserved cryptic epitope in the receptor binding domains of SARS-CoV-2 and SARS-CoV. *Science*. 2020;368(6491):630-633.
18. Ju B, Zhang Q, Ge J, et al. Human neutralizing antibodies elicited by SARS-CoV-2 infection. *Nature*. 2020;584(7819):115-119.
19. Chen P, Nirula A, Heller B, et al. SARS-CoV-2 neutralizing antibody LY-CoV555 in outpatients with Covid-19. *N Engl J Med*. 2021;384(3):229-237.
20. Baum A, Ajithdoss D, Copin R, et al. REGN-COV2 antibodies prevent and treat SARS-CoV-2 infection in rhesus macaques and hamsters. *Science*. 2020;370(6520):1110-1115.
21. Schäfer A, Muecksch F, Lorenzi JCC, et al. Antibody potency, effector function, and combinations in protection and therapy for SARS-CoV-2 infection in vivo. *J Exp Med*. 2021;218(3):e20201993.
22. Piccione EC, Juarez S, Liu J, et al. A bispecific antibody targeting CD47 and CD20 selectively binds and eliminates dual antigen expressing lymphoma cells. *Mabs*. 2015;7(5):946-956.
23. Wu X, Guo J, Niu M, et al. Tandem bispecific neutralizing antibody eliminates HIV-1 infection in humanized mice. *J Clin Invest*. 2018;128(6):2239-2251.
24. De Gasparo R, Pedotti M, Simonelli L, et al. Bispecific IgG neutralizes SARS-CoV-2 variants and prevents escape in mice. *Nature*. 2021;593(7859):424-428.
25. Dong J, Huang B, Wang B, et al. Development of humanized trispecific nanobodies with potent neutralization for SARS-CoV-2. *Sci Rep*. 2020;10(1):17806.
26. Guo J, Zhang J, Du P, et al. Generation and characterization of humanized synergistic neutralizing antibodies against SARS-CoV-2. *J Med Virol*. 2022;94(8):3791-3800.
27. Zheng SQ, Palovcak E, Armache JP, Verba KA, Cheng Y, Agard DA. MotionCor2: anisotropic correction of beam-induced motion for improved cryo-electron microscopy. *Nat Methods*. 2017;14(4):331-332.
28. Rohou A, Grigorieff N. CTFFIND4: fast and accurate defocus estimation from electron micrographs. *J Struct Biol*. 2015;192(2):216-221.
29. Punjani A, Rubinstein JL, Fleet DJ, Brubaker MA. cryoSPARC: algorithms for rapid unsupervised cryo-EM structure determination. *Nat Methods*. 2017;14(3):290-296.
30. Pettersen EF, Goddard TD, Huang CC, et al. UCSF chimera—a visualization system for exploratory research and analysis. *J Comput Chem*. 2004;25(13):1605-1612.
31. Emsley P, Cowtan K. Coot: model-building tools for molecular graphics. *Acta Crystallogr D*. 2004;60(Pt 12 Pt 1):2126-2132.
32. Adams PD, Afonine PV, Bunkóczi G, et al. PHENIX: a comprehensive Python-based system for macromolecular structure solution. *Acta Crystallogr D*. 2010;66(Pt 2):213-221.
33. Anandakrishnan R, Aguilar B, Onufriev AV. H++ 3.0: automating pK prediction and the preparation of biomolecular structures for atomistic molecular modeling and simulations. *Nucleic Acids Res*. 2012;40(Web Server issue):W537-W541.
34. Yan Y, Zhang D, Zhou P, Li B, Huang SY. HDock: a web server for protein-protein and protein-DNA/RNA docking based on a hybrid strategy. *Nucleic Acids Res*. 2017;45(W1):W365-W373.
35. Yurkovetskiy L, Wang X, Pascal KE, et al. Structural and functional analysis of the D614G SARS-CoV-2 spike protein variant. *Cell*. 2020;183(3):739-751.
36. Liu Y, Liu J, Plante KS, et al. The N501Y spike substitution enhances SARS-CoV-2 infection and transmission. *Nature*. 2022;602(7896):294-299.
37. Jangra S, Ye C, Rathnasinghe R, et al. The E484K mutation in the SARS-CoV-2 spike protein reduces but does not abolish neutralizing activity of human convalescent and post-vaccination sera. *medRxiv*.
38. Shang J, Wan Y, Luo C, et al. Cell entry mechanisms of SARS-CoV-2. *Proc Natl Acad Sci*. 2020;117(21):11727-11734.
39. Wang R, Lu J, Chen L, Yu Y, Yang Z. A human bispecific neutralization antibody against four serotypes of dengue virus. *Virology*. 2021;558:49-56.
40. Cao M, Wang C, Chung WK, et al. Characterization and analysis of scFv-IgG bispecific antibody size variants. *Mabs*. 2018;10(8):1236-1247.
41. Brennan M, Davison PF, Paulus H. Preparation of bispecific antibodies by chemical recombination of monoclonal immunoglobulin G1 fragments. *Science*. 1985;229(4708):81-83.
42. Spiess C, Zhai Q, Carter PJ. Alternative molecular formats and therapeutic applications for bispecific antibodies. *Mol Immunol*. 2015;67(2 Pt A):95-106.
43. Lan J, Ge J, Yu J, et al. Structure of the SARS-CoV-2 spike receptor-binding domain bound to the ACE2 receptor. *Nature*. 2020;581(7807):215-220.
44. Focosi D, McConnell S, Casadevall A, Cappello E, Valdiserra G, Tuccori M. Monoclonal antibody therapies against SARS-CoV-2. *Lancet Infect Dis*. 2022;22(11):e311-e326.
45. Shan S, Mok CK, Zhang S, et al. A potent and protective human neutralizing antibody against SARS-CoV-2 variants. *Front Immunol*. 2021;12:766821.
46. Planchais C, Fernández I, Bruel T, et al. Potent human broadly SARS-CoV-2-neutralizing IgA and IgG antibodies effective against Omicron BA.1 and BA.2. *J Exp Med*. 2022;219(7):e20220638.
47. Chi H, Wang L, Liu C, et al. An engineered IgG-VHH bispecific antibody against SARS-CoV-2 and its variants. *Small Methods*. 2022;6(12):e2200932.
48. Wang Y, Zhang X, Ma Y, et al. Combating the SARS-CoV-2 Omicron (BA.1) and BA.2 with potent bispecific antibodies engineered from non-Omicron neutralizing antibodies. *Cell Discov*. 2022;8(1):104.
49. Huang Y, Sun H, Yu H, Li S, Zheng Q, Xia N. Neutralizing antibodies against SARS-CoV-2: current understanding, challenge and perspective. *Antibody Ther*. 2020;3(4):285-299.

SUPPORTING INFORMATION

Additional supporting information can be found online in the Supporting Information section at the end of this article.

How to cite this article: Wang R, Guo J, Lu J, et al. A potential broad-spectrum neutralizing antibody against Betacoronavirus. *J Med Virol*. 2023;95:e29252. doi:10.1002/jmv.29252